Evolution of V-defects and dislocations in InGaN/GaN multi-quantum wells observed by transmission electron microscopy

HUANYOU WANG[a,b,*], GUI JIN[a,b], QIAOLAI TAN[a,c]
[a]*Academy of Electronic Information and Electrical Engineering, Xiangnan University Chenzhou, China*
[b]*School of Information and Optoelectronics Science and Technology, South China Normal University, Guangzhou, China*
[c]*Institute of Physics and Information Science, Hunan Normal University, Changsha, China*

InGaN/GaN multi-quantum well (MQW) structures have been grown on a (0001) sapphire substrate by metalorganic chemical vapor deposition (MOCVD). The origin and evolution of three special V-defects and dislocations are investigated using cross-sectional transmission electron microscopy (TEM) and secondary ion mass spectroscopy (SIMS). Some (a+c) dislocations decompose inside the MQW, resulting in a misfit segment in the c-plane and a V-defect. Some V-defects are generated from the stacking mismatch boundaries induced by stacking faults that are formed within the MQW owing to the strain relaxation. Some V-defects in the MWQ have a thin six-walled structure with InGaN/GaN $\{10\bar{1}1\}$ layers, which is related to the growth kinetics of the GaN crystal and a masking effect of In atoms segregated around the threading dislocation.

(Received September 15, 2017; accepted November 29, 2018)

Keywords: Metal-organic chemical vapor deposition (MOCVD), Patterned sapphire Substrate, Optical emission, Lateral growth

1. Introduction

InGaN/GaN heterostructures and quantum well (QW) structures have a wide range of applications, such as the active layers in GaN-based light-emitting diodes [1, 2]. By controlling the In composition [3, 4], it is possible to tune the optical band gap from the visible to ultraviolet spectral range. However, active III-N layers have a large density of defects that cross the epitaxial layer to depress the device performance [5, 6]. The most detrimental defects in the InGaN/GaN multi-quantum well (MQW) are V-defects or inverted hexagonal pyramid defects. These names originate from the fact that empty pyramidal pits, with hexagonal openings at the growth surface and sidewalls parallel to the $\{10\bar{1}1\}$ planes, are formed during the MQW growth. It is generally believed that the V-defect originates at a threading dislocation (TD) with more probability of nucleation at a mixed TD than at a pure-edge TD [7]. These defects affect the structural and optical qualities of the active layer composed of the InGaN/GaN MQW. Recently, V-defects have received much attention owing to their structures and formation mechanisms. Different structural models have been proposed by X. H. Wu et al. [7-9], such as strain release, low surface mobility of the adatoms on the InGaN layer and/or reduced Ga incorporation on the $\{10\bar{1}1\}$ planes compared with the (0001) surface, have been put forward to explain the generation of these V-defects [10-12]. Theoretical calculations have also been performed to understand the V-defect formation in GaN, such as modelling using first-principles calculations by Northrup and Neugebauer [13] who showed that indium behaves as a differential surfactant.

Despite the above advances, defect-free InGaN/GaN MQW layers have not yet been obtained. The origin of this V-defect and the role it plays on the optical emission are still unclear. This paper correlates the structure and chemistry of the V-defects, using a number of transmission electron microscopy (TEM) techniques to determine their origin and evolution mechanism.

2. Experiment

The green light-emitting diode, studied in this work, was grown on a c-plane sapphire substrate using a VEECO D180 MOCVD system. During the growth, trimethylgallium (TMGa), trimethylindium (TMIn) and ammonia (NH_3) were used as gallium, indium, and nitrogen sources, respectively. Nitrogen was used as a carrier gas for the TMGa and TMIn flows. Silane (SiH_4) and biscyclopentadienyl magnesium (CP_2Mg) were used as the n-dopant and p-dopant source, respectively. After high temperature sapphire cleaning, a thin GaN nucleation

layer was grown at low temperature followed by 2-μm thick un-doped GaN and n-type doped GaN layer growth at 1100 °C. Then, fifteen-period MQWs with 2.5-nm InGaN wells and 12.2 nm GaN barriers were grown. InGaN well growth was performed at 730 °C, while the GaN barrier growth temperature was 840 °C. Finally, a p-AlGaN layer was grown at 950 °C, and a p-GaN layer was grown on the prepared p-AlGaN layer at 1070 °C. The prepared TEM specimens were examined using Philips CM 20 and FEI G2 microscopes operating at 200 kV. The crystal structure and the elemental compositions were analyzed by using FFT analysis of the high-resolution TEM images, energy dispersive X-ray spectroscopy (EDX) and secondary ion mass spectroscopy (SIMS). A Philips MRD high-resolution X-ray diffraction (HRXRD) including a five-crystal monochromator was used for characterization.

3. Results and discussion

Fig. 1 shows the ω–2θ HRXRD patterns at (0002) symmetric planes for the InGaN/GaN MQW. The sharp, well-defined satellite peaks show excellent layer crystalline perfection and sharp interfaces between all multiple layers. The sharp dominant peak is attributed to (0002) of the 2-μm-thick n-GaN film and the broader peak at lower angle arises from the (0002) diffraction from InGaN/GaN MQW and this is labeled as the zeroth-order peak. Using the X'Pert Epitaxy simulation software, from fitting of the HRXRD scan at (0002) plane, the well/barrier width and average indium composition were estimated to be approximately 2.5 nm, 12.2 nm and 19.6% for InGaN/GaN MQWs.

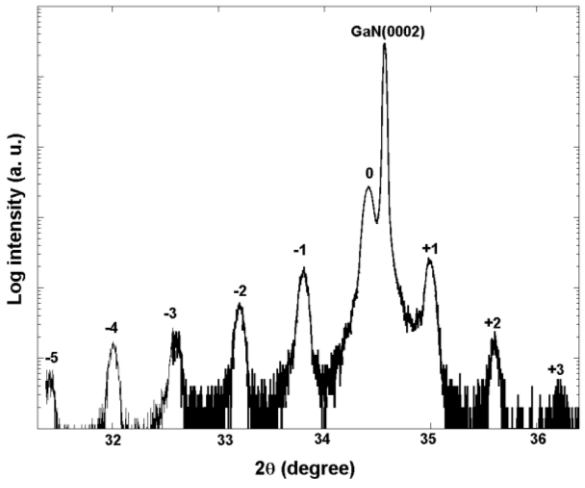

Fig. 1. The double crystal X-ray ω–2θ scan spectra of (0002) planes of a InGaN/GaN MQW

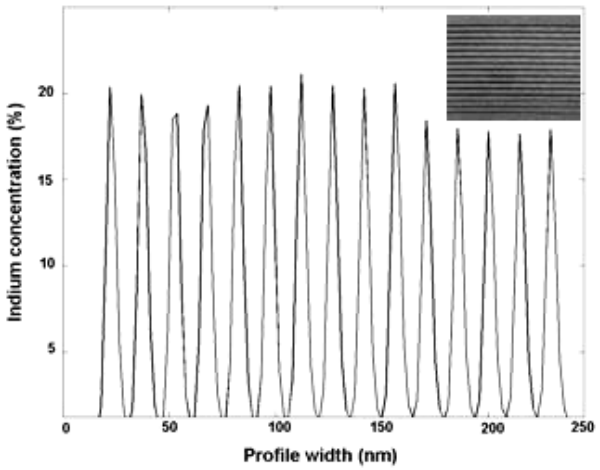

Fig. 2. The SIMS micrograph of indium concentration across the MQW. The upper right corner is Cross-section TEM image of the InGaN/GaN MQW

Fig. 2 shows t the SIMS micrograph of indium concentration across the MQW. Fifteen QW can be clearly identified in the image. The measured well and barrier widths were in good agreement with the HRXRD simulation. A nitrogen/gallium elemental ratio-map was used to give an accurate measure of the indium concentration across the MQW layers (19.7±3%) based on the assumption that the nitrogen concentration remains constant throughout the structure. A compositional line-trace calculated in this way is shown in Fig. 2, showing a small variation in the indium concentration across the MQW. The results from SIMS and TEM show that the In concentration decreases slightly in the MQW layers from bottom to top, which suggests that during growth, the cumulative strain due to lattice mismatch between GaN and InGaN reduces the In incorporation. In addition, the samples were grown with an In concentration of 20%, which was relatively higher and might lead to inhomogeneity.

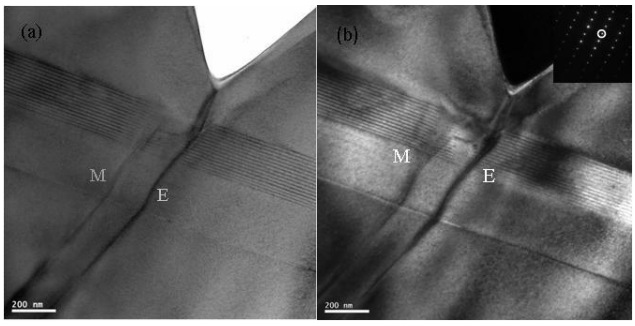

Fig. 3. Cross-section bright field TEM image of the InGaN/GaN MQW taken from (a) g=(0002) and dark field TEM image taken from (b) g= $(1\bar{1}00)$ *. The diffraction spot (marked in upper right corner of (b)) was used for the bright field and dark field*

Fig. 3 is the cross-section bright-field and dark-field TEM image of the MQW heterostructure. A mixed-type threading dislocation (marked with M) and a pure-edge TD (marked with E) are seen in the micrograph. The mixed-type threading dislocation decomposed an *a*-type and a *c*-type dislocation. The *a*-type component dislocation bends to an interfacial direction leading to a misfit dislocation in the InGaN/GaN interface, and subsequently from an interfacial to a threading dislocation again. The *c*-type component dislocation is not seen owing to the $g \cdot b$ invisibility criteria, and the decomposition reaction is an energetically neutral reaction [14]. This dislocation has a Burgers vector $b = 1/3\langle 11\bar{2}0 \rangle$ in the $\{0001\}$ slip plane and relieves the mismatch in that area. Owing to the poor miscibility between GaN and InN, In-rich clusters have been detected inside the InGaN quantum wells, which result from indium composition fluctuations [15, 16]. The In compositional fluctuation inside the quantum well may give rise to the decomposition reaction of this threading dislocation, and thereby can generate a misfit strain-induced dislocation. The threading dislocations associated with this kind of defect can have different characters, with an increased nucleation possibility when the dislocation has a *c*-component [7]. The In distributions along the quantum wells have been detected with SIMS. The measurement result is shown in Fig. 2, and the measured value was almost 20%. Thus, the local strain may be very high and a small critical layer thickness may be evident, which should explain the bending of the dislocation with an *a*-component from threading to a misfit segment dislocation. Then, the combination of an a-type and a *c*-type to form a new dislocation with (a+c) Burgers vector has been reported in GaN epitaxy grown on sapphire [14] and 6H-SiC [17]. Then, the local In fluctuations will cause the misfit dislocation to impact with regions where the local In concentrations happen to be quite low. The boundary between the highly strained areas and unstrained areas will then offer a driving force for the dislocation to climb back to the (0001) direction. Therefore, we can distinguish three different areas: the incident mixed (a+c) threading dislocation arriving onto the MQW heterostructure; an *a*-component misfit dislocation in the basal plane; and an edge threading dislocation running up from the heterostructure.

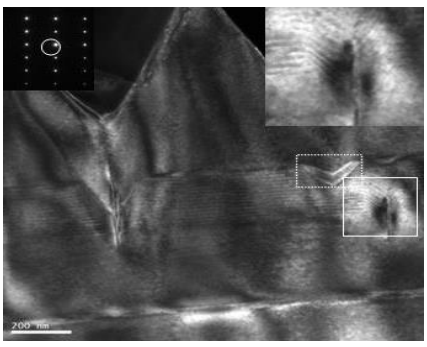

Fig. 4. Cross-sectional dark field TEM image of the InGaN/GaN MQW taken from g=(0002). Top right corner is magnified image from the solid rectangle. The diffraction spot (marked in the upper left corner) was used

Fig. 4 is a cross-sectional dark field TEM image of the InGaN/GaN MQW, which shows that V-defects originate from not only TDs but also other sites (as marked by the dashed rectangle). The V-defect in the dashed rectangle is initiated at the upper interface of the InGaN/GaN, and is not related to the propagation of TDs. A frequently observed V-defect in the InGaN/GaN heterostructure starts on TDs, which run from the high temperature GaN layer to the capping layer through the MQW. The V-defect in the dashed rectangle can mainly be connected with the stacking faults in the InGaN/GaN heterostructure. To determine the origin of the V-defects in relation to the stacking fault, the high resolution bright field TEM image is shown in Fig. 5. In Fig. 5, the thickness of the well under the V-defect is higher than the thickness of the surrounding well, and the V-defect is initiated at the upper interface of the InGaN/GaN.

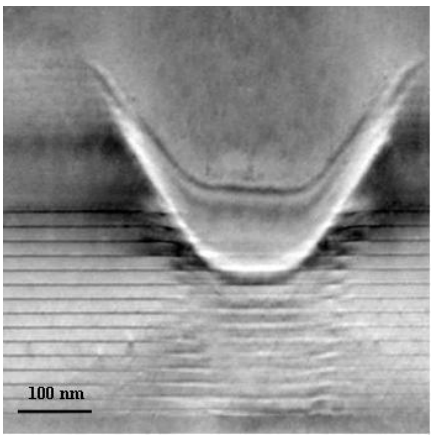

Fig. 5. Cross-sectional high resolution bright field TEM image of the InGaN/GaN MQW. The V defect is initiated at upper interface of the InGaN/GaN

It has been reported that in the InGaN/GaN heterostructure, stacking faults are easily formed in the GaN layer owing to the shear in the less compliant GaN layer and a low formation energy of stacking faults of only ~20 meV [18], and stacking faults can relax the large strain in the InGaN/GaN MQW of high In composition. Although the strain may play a central role in the nucleation of the V-defect, the strain relief should not be the main cause of the V-defect growth (note that the mismatch between GaN and InN is ~12% in both the a and c directions). Rather, the reduced Ga incorporation (and thus the growth rate) on the pyramid planes compared with (0001) planes is the primary cause for V-defect growth. In normal InGaN/GaN MQW growth, owing to the low sticking coefficient of In atoms at a high growth temperature, the GaN barrier growth temperature is ~250 °C lower than that used in high-temperature GaN growth to suppress re-evaporation of In. In this temperature regime, there is poor surface migration of gallium on the

$\{0001\}$ surface, which deteriorates the layer-by-layer growth. Meanwhile, In atoms are trapped and segregated in the strained field around the core of a TD. The formation of these pits has an important relation to the growth kinetics of the InGaN layer. Increasing the composition of In in the InGaN well enhances pits generation with a higher strain between the well and the barrier interface. Modeling by Northrup et al. [13], using first-principles calculation, has shown that indium acts as a differential surfactant in reducing the surface energy of $\{10\bar{1}1\}$ facets as compared with that of the $\{0001\}$ plane. That is, the stacking order of *ABABABAB* along the *c* axis is transformed into that of *ABABCBCB* in the faulted area. These promote V-defects generation with $\{10\bar{1}1\}$ opening out from the threading dislocations into the subsequent interlayers of InGaN/GaN. That is, adatoms migrate out of the pits and incorporate in the adjacent areas during growth. Since the area consumed by pits increases toward the top of the stack, the growth rate outside of them increases continually. While the MQW layers can be very rough, the pits planarize rapidly during subsequent growth of the p-type layers. Final surfaces typically show no evidence of pitting in Fig. 5.

In Fig. 4, the V-defects in the solid rectangle include several obvious stripes parallel to the $\{10\bar{1}1\}$ sidewalls, which is clearly connected to a TD. It is estimated from TEM that the angle between the $(10\bar{1}1)$ and $(\bar{1}011)$ facets is approximately 55°, which is close to the theoretical value of 56.1°. The inclined brighter thin stripes terminate on a horizontal InGaN QW, and the corners connecting the $(10\bar{1}1)$ interface (or $(\bar{1}011)$ interface) with the (0001) interface are not sharp, but curved, as shown in the magnified image in the top right corner of Fig. 4. The InGaN and GaN sidewall layers were epitaxially grown successively on the six $\{10\bar{1}1\}$ planes during the MQW deposition, which is similar to the growth on the (0001) planes by the layer-by-layer growth. The stripes parallel to the $\{10\bar{1}1\}$ sidewalls of the V-defects correspond with the models of X. H. Wu and K. Watanabe [8]. Recently, Shiojiri et al. [19] have also studied the formation mechanism of V-defects by analyzing the growth kinetics of the GaN crystal in view of the masking effect of In atoms with analogy to epitaxial lateral overgrowth. As mentioned above, the mask induces V-defects in quantum wells and barriers to the growth of exposed $\{10\bar{1}1\}$ surfaces at low temperatures, while the (0001) growth on the surface is not a masking effect. Thus, the whole MWQ has the (0001) surface as well as the $\{10\bar{1}1\}$ surfaces during the MQW deposition. The InGaN and GaN crystals on the (0001) and $\{10\bar{1}1\}$ surfaces were grown by the layer-by-layer method. When the monolayers are grown, the supply of atoms on both the (0001) and $\{10\bar{1}1\}$ surfaces is gradually reduced, and the InGaN growth rate is smaller than that of the GaN. Before they meet with each other, the monolayers on the (0001) and $\{10\bar{1}1\}$ surfaces can cease from growing. However, they exhibit a low growth rate at the low temperature of 800 °C. With the successive growth of these monolayers, a surface with step-wise lattices was formed near the corner.

4. Conclusions

Fifteen periods of InGaN/GaN MQW with sharp interfaces have been grown by atmospheric pressure MOCVD. In summary, we have reported the formation of V-defects in InGaN/GaN MQW. In the MQW, (a+c)-type dislocations can decompose, and they give rise to V-defects and misfit segments that locally relieve the strain, probably owing to the local In composition fluctuations as confirmed by SIMS. V-defects originate not only from TDs but also from other sites, and this V-defect can be mainly connected with stacking faults in the InGaN/GaN heterostructure. The stacking faults are easily formed in the GaN layer owing to the shear in the less compliant GaN layer and low formation energy. The InGaN and GaN sidewall layers were epitaxially grown successively on the six $\{10\bar{1}1\}$ planes during the MWQ deposition, which is similar to the growth on the (0001) planes by the layer-by-layer growth. This can be explained by analyzing the growth kinetics of the GaN crystal and the masking effect of In atoms by analogy with epitaxial lateral overgrowth.

Acknowledgment

This work was supported by Science Foundation of Education Department of Hunan Provincial (Grant No. 10C1235), the Natural Science Foundation of Hunan Province (Grant No. 13JJ3121).

References

[1] S. Nakamura, S. Fasol, The Blue Laser Diode, Springer, Berlin, 1997.
[2] L. Cheng, S. Wu, C. Xia, H. Chen, J. Appl. Phys. **118**, 103103 (2015).
[3] A. M. Armstrong, B. N. Bryant, M. H. Crawford, D. D. Koleske, S. R. Lee, J. Appl. Phys. **117**, 134501 (2015).
[4] S. W. Hwang, B. Lee, S. H. Choi, J. Korean Phys. Soc. **69**, 772 (2016).
[5] L. C. Le, D. G. Zhao, D. S. Jiang, L. Li, L. L. Wu, J. Appl. Phys. **114**, 143706 (2013).
[6] C. Bazioti, E. Papadomanolaki, T. Kehagias, T. Walther, J. Smalckoziorowska, J. Appl. Phys. **118**, 132117 (2015).
[7] X. H. Wu, C. R. Elsass, A. Abare, M. Mack, S. Keller, P. M. Petroff, S. P. Den Baars, J. S. Speck, Appl. Phys. Lett. **72**, 692 (1998).
[8] K. Watanabe, J. R. Yang, S. Y. Huang, K. Inoke, J. T. Hsu, R. C. Tu, T. Yamazaki, N. Nakanishi, M. Shiojiri, Appl. Phys. Lett. **82**, 718 (2003).

[9] N. Sharma, P. Thomas, D. Tricker, C. Humphreys, Appl. Phys. Lett. **77**, 1274 (2000).
[10] J. Smalckoziorowska, E. Grzanka, R. Czernecki, D. Schiavon, M. Leszczyński, Appl. Phys. Lett. **106**, 101905 (2015).
[11] A. V. Lobanova, A. L. Kolesnikova, A. E. Romanov, S. Y. Karpov, M. E. Rudinsky, Appl. Phys. Lett. **103**, 152106 (2013).
[12] H. Y. Wang, X. C. Wang, Q. L. Tan, X. H. Zeng, Materials Science in Semiconductor Processing, **29**, 112 (2015).
[13] J. E. Northrup, J. Neugebauer, Phys. Rev. B. **60**, R8473 (1999).
[14] F. R. Chien, X. J. Ning, S. Stemmer, P. Pirouz, M. D. Bremser, R. F. Davis, Appl. Phys. Lett. **68**, 2678 (1996).
[15] P. Ruterana, S. Kret, A. Vivet, G. Maciejewsk, P. Dluzewski, J. Appl. Phys. **91**, 8979 (2002).
[16] D. Gerthsen, E. Hahn, B. Neubauer, A. Rosenauer, O. Schon, M. Heuken, A. Rizzi, Phys. Status Solidi, A Appl. Res. **177**, 145 (2000).
[17] F. R. Chien, X. J. Ning, S. Stemmer, P. Pirouz, M. D. Bremser, R. F. Davis, Appl. Phys. Lett. **68**, 2678 (1996).
[18] L. T. Romano, B. S. Krusor, R. J. Molnar, Appl. Phys. Lett. **71**, 2283 (1997).
[19] S. K. Julita, G. Ewa, C. Robert, S. Qario, L. Mike. Appl. Phys. Lett. **106**, 101905 (2015).

*Corresponding author: whycs@163.com